

# Photonic Non-Abelian Braid Monopole

Kunkun Wang,<sup>1,2,\*</sup> J. Lukas K. König,<sup>3,\*</sup> Kang Yang,<sup>4</sup> Lei Xiao,<sup>2</sup> Wei Yi,<sup>5,6</sup> Emil J. Bergholtz,<sup>3,†</sup> and Peng Xue<sup>7,2,‡</sup>

<sup>1</sup>*School of Physics and Optoelectronic Engineering, Anhui University, Hefei 230601, China*

<sup>2</sup>*School of Physics, Southeast University, Nanjing 211189, China*

<sup>3</sup>*Department of Physics, Stockholm University, AlbaNova University Center, 106 91 Stockholm, Sweden*

<sup>4</sup>*Dahlem Center for Complex Quantum Systems and Fachbereich Physik,  
Freie Universität Berlin, 14195 Berlin, Germany*

<sup>5</sup>*Key Laboratory of Quantum Information, University of Science and Technology of China, CAS, Hefei 230026, China*

<sup>6</sup>*CAS Center for Excellence in Quantum Information and Quantum Physics,  
University of Science and Technology of China, Hefei 230026, China*

<sup>7</sup>*Beijing Computational Science Research Center, Beijing 100084, China*

Monopoles and braids are exotic but elusive aspects of fundamental theories of light and matter. In lattice systems, monopoles of band-structure degeneracies are subject to well-established no-go (doubling) theorems that appear to universally apply in closed Hermitian systems and open non-Hermitian systems alike. However, the non-Abelian braid topology of non-Hermitian multi-band systems provides a remarkable loophole to these constraints. Here we make use of this loophole, and experimentally implement, for the first time, a monopole degeneracy in a non-Hermitian three-band system in the form of a single third-order exceptional point. We explicitly demonstrate the intricate braiding topology and the non-Abelian fusion rules underlying the monopole degeneracy. The experiment is carried out using a new design of single-photon interferometry, enabling eigenstate and spectral resolutions for non-Hermitian multi-band systems with widely tunable parameters. Thus, the union of state-of-the-art experiments, fundamental theory, and everyday concepts such as braids paves the way toward the highly exotic non-Abelian topology unique to non-Hermitian settings.

## I. INTRODUCTION

Monopoles enjoy recurring interest in high-energy physics, following Dirac’s observation that a magnetic monopole ties the quantisation of electric charge to that of angular momentum throughout the universe [1]. Monopoles arise as particularly exotic particles in the search for a Grand Unified Theory, motivating continued efforts in simulating their counterparts in lower-energy physics. However, these efforts are often thwarted by the famous Nielsen-Ninomiya fermion-doubling theorem [2, 3], which asserts that charges carried by particles often have to be compensated, thus obstructing the occurrence of monopoles.

One caveat of the fermion-doubling theorem is that it requires simply additive charges, such that its traditional form does not apply to non-Abelian charges. Such non-Abelian particles, often called anyons, obey non-commuting statistics and follow path-dependent fusion rules. Since non-Abelian fusion outcomes can only be modified by topologically robust braiding operations, non-Abelian charges are considered useful for applications in error-proof information storage and manipulation [4].

Despite their theoretical significance and potential wide applications, implementing non-Abelian monopoles and fusion processes remains challenging. Dissipative

systems promise to close this experimental gap. Band crossings in such systems are generically twofold exceptional points (EP2s) [5, 6], which have various practical applications ranging from topological energy transfer in optomechanical systems, to the enhancement of sensitivity [7–14].

The non-Abelian nature of these EP2s arises from complex-valued “energies”, which reflects the dissipation of the underlying systems. These energies braid around each other near the EP2s, endowing each of them with a braid topological invariant. Intriguingly, these braids are non-Abelian for systems of more than two bands [15–24], which opens up the possibility of circumventing fermion-doubling and constructing braid-protected monopoles in multi-band dissipative systems [25]. While dissipation is ubiquitous in photonic, mechanic, and electric-circuit systems [26–31], observation and manipulation of monopoles and non-Abelian phenomena remain elusive, for want of a suitably tunable dissipative system.

In this work, we report on the experimental creation and manipulation of a non-Abelian monopole and EP2s in a single-photon interferometric network (Fig. 1), and tune their movement along non-trivial paths. Distinct from previous studies [32–35], for the first time we control and observe the fusion of EP2s, which either results in gap-opening or a non-Abelian monopole depending on the topology of their preceding paths. We further demonstrate that non-Hermitian phase transitions are triggered by moving EP2s along such non-trivial paths. This clearly shows the non-Abelian nature of our setup. Compared to non-Abelian phenomena in many-body sys-

---

\* These authors contributed equally to this work

† [emil.bergholtz@fysik.su.se](mailto:emil.bergholtz@fysik.su.se)

‡ [gnepeux@gmail.com](mailto:gnepeux@gmail.com)

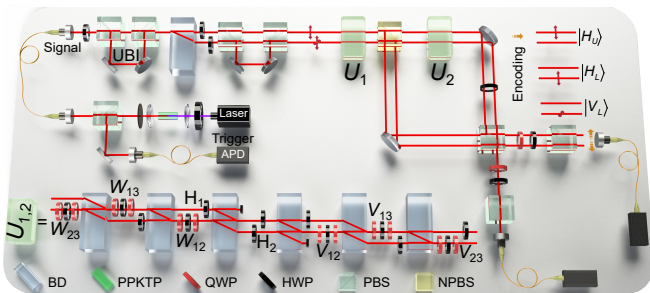


FIG. 1. Experimental setup. We generate photon pairs, consisting of trigger and signal photon, via type-II spontaneous parametric down-conversion through a periodically poled potassium titanyl phosphate (PPKTP) crystal. In the state space spanned by horizontally polarised light in the upper spatial mode  $|HU\rangle$ , lower spatial mode  $|HL\rangle$ , and vertically polarised lower spatial mode  $|VL\rangle$ , we prepare the signal photon in a completely mixed qutrit state through two unbalanced interferometer (UBI) setups, consisting of four polarizing beam splitters (PBSs), three half-wave plates (HWPs) and a beam displacer (BD). We purify this mixed state into one of the eigenstates of the non-Hermitian Hamiltonian  $H$  by way of a non-unitary operation  $U_1$ , realized by six BDs interspersed with HWPs and quarter wave-plates (QWPs). To measure the associated eigenvalue, we split the photon beams with a non-polarizing beam splitter (NPBS), and let the transmitted photons evolve under non-unitary  $U_2$  governed by  $H$ . They acquire a complex phase shift relative to the beams reflected in the NPBS, which corresponds to the eigenvalues of  $H$ . We measure these eigenvalues interferometrically, using avalanche photodiodes (APDs), by detecting coincidences between the signal and trigger photons.

tems [36] and Hermitian non-interacting systems [37–39], our setup does not require fine-tuned interactions or additional symmetries – instead it relies on the topological robustness of braids.

## II. NON-ABELIAN MONOPOLE IN PHOTON INTERFEROMETRY

We implement a non-unitary evolution of photons according to a 3-level Hamiltonian

$$H_M^\delta = \begin{pmatrix} \delta - e^{ik_x} & -i(1 + e^{ik_x}) & 0 \\ -i(1 + e^{ik_x}) & e^{ik_x} - e^{ik_y} & -i(1 + e^{ik_y}) \\ 0 & -i(1 + e^{ik_y}) & -\delta + e^{ik_y} \end{pmatrix}. \quad (1)$$

This models the Bloch Hamiltonian of a two-dimensional lattice system with three orbitals per unit cell. The  $2\pi$ -periodicity in both quasimomenta  $k_x$  and  $k_y$  thus parameterises the vector  $\mathbf{k} = (k_x, k_y)$  on a Brillouin zone (BZ) torus. For  $\delta = 1 + 2\sqrt{2}$  the system contains the monopole, a single non-trivial degenerate point, at  $k_x = k_y = 0$  (see Fig. 2 (a)).

Experimentally we simulate Eq. (1) on a qutrit state space of hybrid polarisation-spatial modes of single photons using the setup shown in Fig. 1. Specifically, we encode the three basis states in the horizontal polarisation

of the photons in the upper and lower spatial modes, and the vertical polarisation in the lower mode, respectively.

To spectrally resolve the monopole and the non-Abelian braid, we devise a three-step protocol to distill the eigenstates from a completely mixed state and subsequently obtain the complex spectrum from single-photon interferometry. First, we prepare the completely mixed qutrit state by subjecting the single photon successively to a pair of unbalanced interferometers (see Methods). We subsequently implement imaginary-time evolution for a time  $\tau_1$  under a suitably chosen operator  $U_1 = e^{f_j(H)\tau_1}$  that damps all but the  $j$ -th eigenstate of  $H(\mathbf{k})$  [40, 41]. Through appropriate choice of  $f_j(H)$ , any eigenstate can be distilled in this manner. Finally, we obtain the corresponding complex eigenvalue to the prepared eigenstate by letting the system evolve in real time under  $U_2 = e^{-i(H-i\Lambda\mathbb{1})\tau_2}$  and measuring the resulting states interferometrically (see Methods). Here we introduce the parameter  $\Lambda$ , mapping the evolution to a passive operation, and thus bypassing the obstacle of achieving coherent gains in quantum systems. We repeat the above measurements for a given Hamiltonian  $H_M^\delta(\mathbf{k})$  at representative quasimomenta  $\mathbf{k} = (k_x, k_y)$  throughout the BZ to resolve the complex spectrum of the three-band system.

For  $\delta = 1 + 2\sqrt{2}$  the monopole at  $k_x = k_y = 0$  is experimentally confirmed through spectral measurement, as illustrated in Fig. 2 (b). Only at the monopole, all three eigenvalues merge to  $E_{1,2,3} = 0$ . While the existence of the monopole contrasts conventional fermion-doubling theorems [2, 3, 42], we can understand its occurrence by measuring its dispersion, which gives the braid topological invariant protecting it. Near the monopole, the absolute values of the spectrum in general disperse as  $|\delta E| \sim |\delta k|^{1/3}$ . However, their complex phases have a strong dependence on the direction from which the monopole is approached. Following a loop that encloses the monopole, the complex eigenvalues thus wind around each other and form a non-trivial braid  $B_M$ . We thus call the monopole a braid monopole, or, since the braid group is non-Abelian, a non-Abelian monopole. Expressed in terms of simple counterclockwise two-level braiding of energies  $\sigma_i$ , this braid is  $B_M = \sigma_1\sigma_2\sigma_1^{-1}\sigma_2^{-1}$  (see Fig. 2 (c)).

The braid  $B_M$  associated to the monopole is invariant under deformations of the loop [15, 16, 20]. Therefore we obtain the same braid pattern when measured along the boundary of the BZ [43, 44] (see Fig. 2 (d)). For Bloch Hamiltonians, this boundary consists of meridian and longitude circles around the Brillouin zone torus. These circles carry braids  $B_{x,y}$  individually, so the monopole braid splits into four parts,

$$B_M = B_x B_y B_x^{-1} B_y^{-1}. \quad (2)$$

This is at the heart of Fermion doubling; for Abelian invariants these four parts would commute, resulting in  $B_x B_x^{-1} B_y B_y^{-1} = 1$ , so topological Abelian monopoles cannot exist. In comparison, Eq. (2) illustrates the loop-hole we utilise here: for non-Abelian braid invariants this

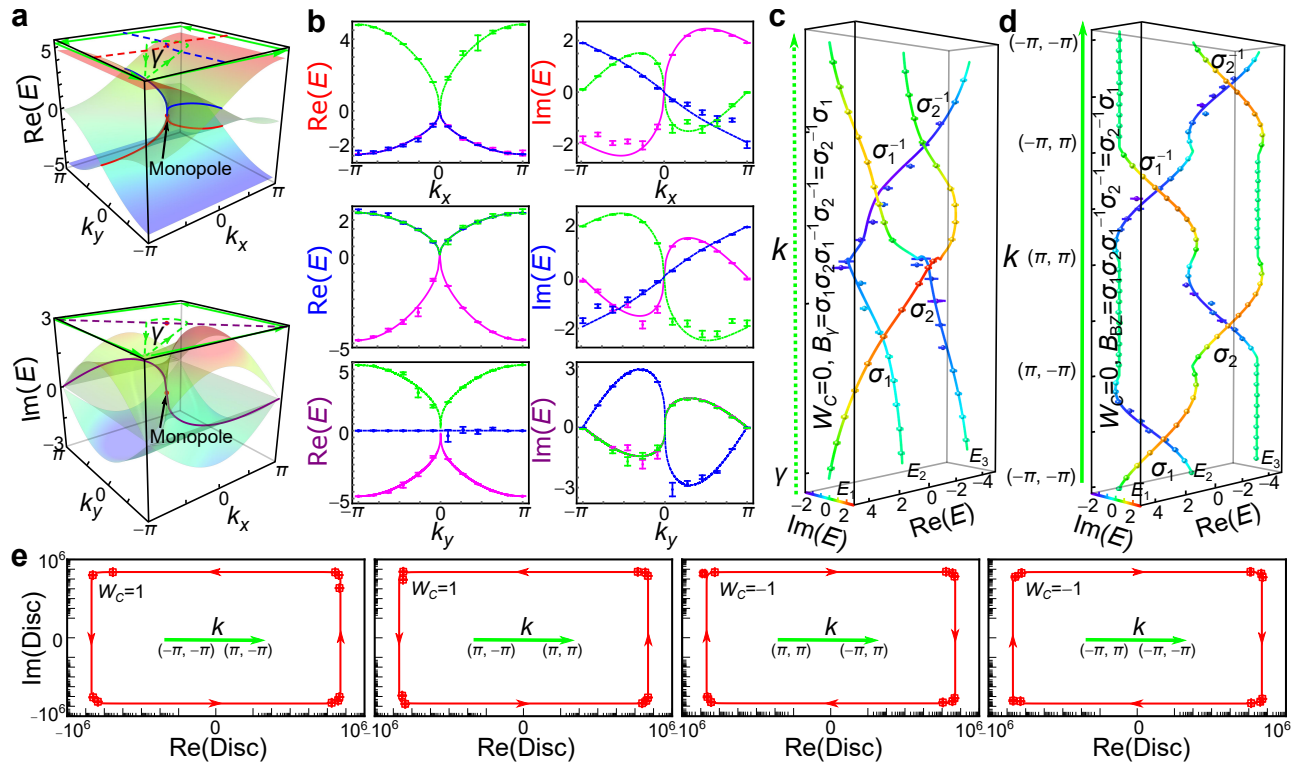


FIG. 2. Observation of the Non-Abelian Monopole. (a) Theoretical results for real and imaginary parts of the spectrum of  $H_M^{\delta=1+2\sqrt{2}}$ , as defined in Eq. (1). The red dot marks the non-Abelian monopole. The solid lines depict the Fermi-arcs of the real spectral components and i-Fermi-arcs of the imaginary components, respectively. The dashed lines are their projections to the  $k_x$ - $k_y$  plane. The path  $\gamma$  encircles the monopole and has  $k_x = k_y = -\pi$  as its base point. (b) The measured eigenvalues along the real and imaginary (i-)Fermi-arcs shown in (a), illustrating the point-like nature of the monopole and its dispersion. (c) The measured braid along the loop  $\gamma$  corresponds to braid word  $B_\gamma = \sigma_1\sigma_2\sigma_1^{-1}\sigma_2^{-1}$ . (d) The loop following the Brillouin zone boundary is homotopy equivalent to  $\gamma$  and thus carries the same braid. (e) Measured discriminant (see Eq. (3)) for the four segments of the loop shown in (c). Each overcrossing (undercrossing) contributes a winding of  $W = +1$  ( $W = -1$ ) of this discriminant around the origin. The total winding is  $W_{BZ} = 0$ , in accordance with the Abelianized sum rule. Experimental data are represented by dots with error bars, theoretical results are denoted by continuous lines. The error bars indicate statistical uncertainty, obtained by assuming Poisson statistics in the photon-number fluctuations.

argument fails. Specifically, for the non-Hermitian three-band model (1), we identify the boundary invariants  $B_x = \sigma_1, B_y = \sigma_2$  (see Fig. 2 (d)). These do not commute, thus enabling a topologically non-trivial monopole protected by braid invariant  $B_M = \sigma_1\sigma_2\sigma_1^{-1}\sigma_2^{-1}$ .

In Fig. 2 (e), we highlight this difference to Abelian two-level systems [18, 21, 42, 45], by showcasing the degree of the monopole braid, an Abelian invariant that can be derived from a braid. It can be obtained by counting the number of strand exchanges, taking their direction into account but disregarding which bands are involved. This reduction corresponds to the Abelianisation of the three-strand braid group  $\mathbb{B}_3/\mathbb{B}_3 = \mathbb{Z}$  [20, 25]. We can equivalently express it in terms of the discriminant

of the characteristic polynomial [19, 20, 42],

$$\begin{aligned} \frac{\mathbb{B}_3}{[\mathbb{B}_3, \mathbb{B}_3]} : W_C &= \sum_{i \neq j} \frac{1}{2\pi} \oint_C \partial_{\mathbf{k}} \arg [E_i(\mathbf{k}) - E_j(\mathbf{k})] d\mathbf{k} \\ &= \frac{1}{2\pi i} \oint_C \partial_{\mathbf{k}} \ln \text{disc}[H(\mathbf{k})] d\mathbf{k}. \end{aligned} \quad (3)$$

The discriminant  $\text{disc}[H(\mathbf{k})] = \prod_{i < j} [E_i(\mathbf{k}) - E_j(\mathbf{k})]^2$  is a non-zero complex number for non-degenerate matrices, and the braid degree is its winding number from the fundamental group of the punctured complex plane  $W_C \in \pi_1(\mathbb{C} - \{0\}) = \mathbb{Z}$ . As the Abelian part of the eigenvalue braid,  $W_C$  must vanish when following the boundaries of the BZ (see Fig. 2 (e)) [42]. However, the full non-Abelian braid is not trivial [25] such that the nodal phase remains protected and cannot be destroyed perturbatively.

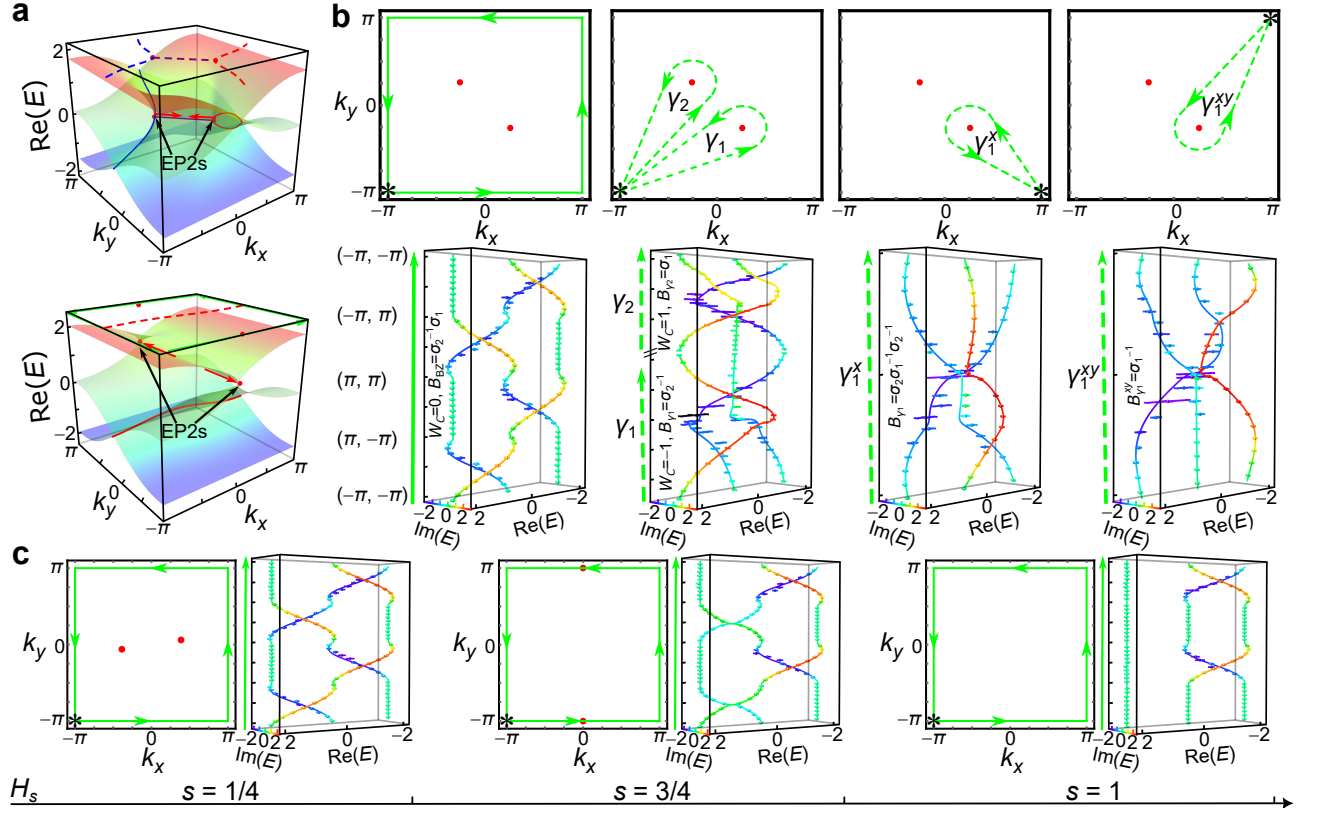


FIG. 3. Path-dependent fusion. (a) Theoretical results for real and imaginary parts of the spectra, shown as colored surfaces over the Brillouin zone (BZ). The red dots correspond the EP2s. Top:  $H_M^{\delta=1} = H_{s=0}$ . The EP2s locally fuse to the braid monopole (see Fig. 2) and cannot be gapped out. Bottom:  $H_M^{\delta=1} = H_{s=3/4}$ . Fusing the EP2s on the edge of the BZ they annihilate and gap out, decoupling the top band. (b) Panel 1, top: Parametric loop along the BZ boundary based at  $(k_x, k_y) = (-\pi, -\pi)$ . Panel 1, bottom: Eigenvalue braid of  $H_M^{\delta=1}$  along this loop. Theoretical predictions in solid lines, experimental data in points. Error bars indicate statistical uncertainty assuming Poisson statistics in the photon-number. The braid along the BZ boundary remains the same compared to the monopole system measured in Fig. 2. Panel 2: as panel 1. The individual EP2s carry braid invariants  $B_{\gamma_1} = \sigma_2^{-1}$  and  $B_{\gamma_2} = \sigma_1$ . Panel 3: as panel 1. Shifting the base point of loop  $\gamma_1$  by  $\Delta k_x = 2\pi$  changes the braid by a non-Abelian conjugate action, resulting in  $B_{\gamma_1^x} = B_x^{-1} B_{\gamma_1} B_x = \sigma_1^{-1} \sigma_2^{-1} \sigma_1 = \sigma_2 \sigma_1^{-1} \sigma_2^{-1}$ . Panel 4: as panel 1. Subsequently shifting the base point by  $\Delta k_y = 2\pi$  leads to  $B_{\gamma_1^{xy}} = B_y^{-1} B_{\gamma_1^x} B_y = \sigma_1^{-1}$ . (c) Further perturbing the system along  $H_s$  moves the EP2s across the boundary, fusing them after they followed a non-trivial loop around the torus. This changes the boundary braid to  $B_{BZ} = 1 \sigma_2 \sigma_1^{-1} = 1$ .

### III. NON-ABELIAN FUSION

A natural question is how this monopole emerges from more conventional non-Hermitian band structures. As we will see, the existence of a monopole under periodic boundary condition is the consequence of path-dependent fusion rules. The high level of control over our optical setup allows us to observe the fusion and decomposition of EPs.

Detuning to  $\delta < 1 + 2\sqrt{2}$ , the system cannot gap out since the monopole is topological. Instead, it decomposes into a pair of twofold EP2s (see Fig. 3). Importantly, these EP2s in our three-band system are non-Abelian, and cannot locally pairwise annihilate, in contrast to their counterparts in two-band models [25]. As a hallmark of this non-Abelian structure, we measure the braid invariants for the same EP along topologically dif-

ferent enclosing loops. Shifting a loop  $\gamma$  encircling the EP by another loop  $\phi$  is associated with a conjugate action  $B_\gamma \rightarrow B_\phi^{-1} B_\gamma B_\phi$  [46] on the charge of the EP. We experimentally confirm this dependence for a loop encircling one of the exceptional points in Fig. 3 (b). Taking  $k_x = k_y = -\pi$  as the base point, this exceptional point corresponds to the braid  $B_{\gamma_1} = \sigma_2^{-1}$ . Shifting to a loop based at  $k_x = +\pi$ , we find braid  $B_{\gamma_1^x} = \sigma_2 \sigma_1^{-1} \sigma_2^{-1}$ , while for base point  $k_x = k_y = +\pi$ , we find  $B_{\gamma_1^{xy}} = \sigma_1^{-1}$ .

The difference between these loops is a shift by a meridian or longitude around the torus. Correspondingly, the movement of EP2s encircling these torus handles leads to different fusion results, further highlighting their non-Abelian structure. In the following, we illustrate this on the pair of EP2s that locally emerge from the monopole. After splitting the monopole into two EP2s, ending at  $H_M^{\delta=1}$ , with the two EP2s at  $(k_x, k_y) \approx \pm(0.815, -0.815)$ ,

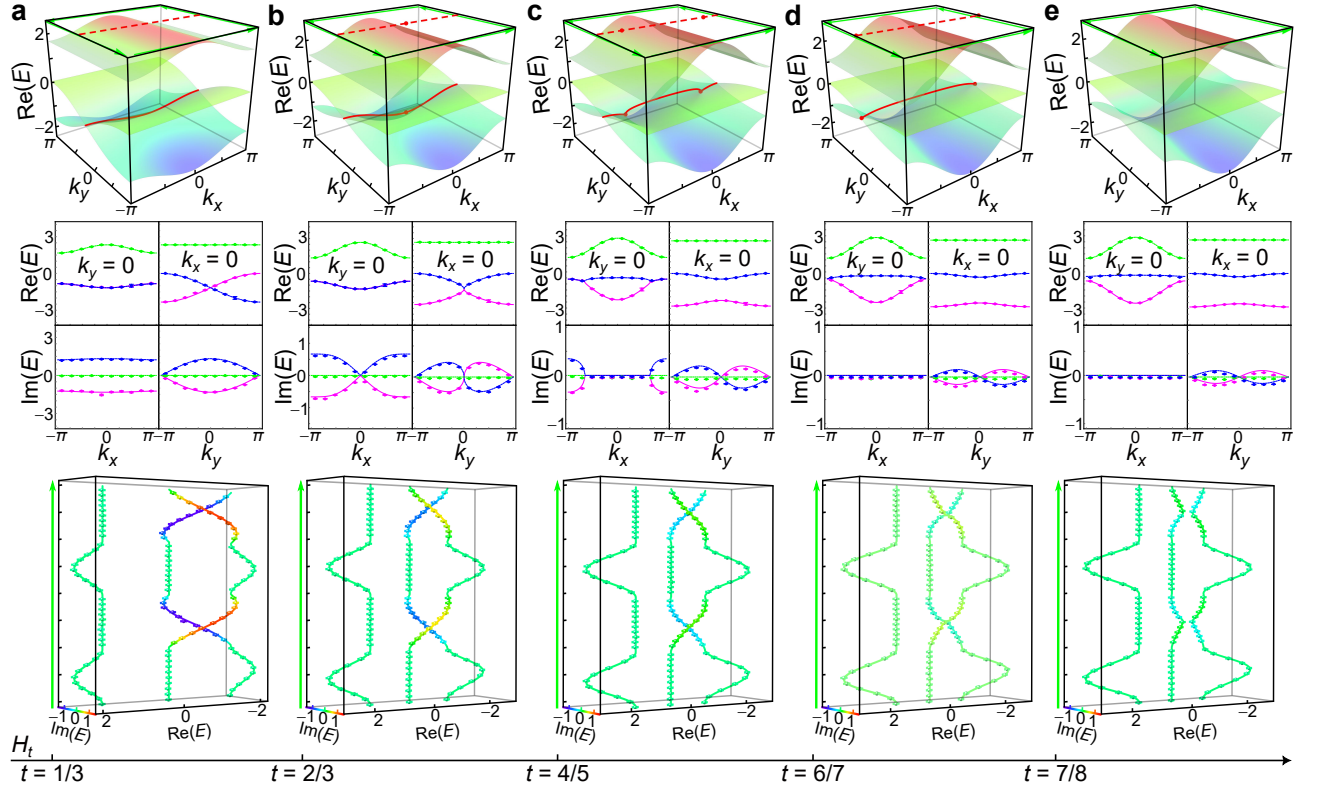


FIG. 4. Topological transition between different band-gapped phases via creation and annihilation of a pair of EP2s. Eigenvalues of  $H_t$  for (a)  $t = 1/3$ , (b)  $t = 2/3$ , (c)  $t = 4/5$ , (d)  $t = 6/7$ , (e)  $t = 7/8$ , respectively. Continuous lines and surfaces correspond to theoretical predictions, measurements are represented by dots; error bars indicate the statistical uncertainty, obtained by assuming Poisson statistics in the photon-number fluctuations. Top: The coloured surfaces depict real parts of the eigenvalues over the Brillouin zone (BZ). The solid lines correspond to the Fermi arcs, the dashed lines to their projection. Middle: Real and imaginary parts of the eigenvalues for  $k_y = 0$  and  $k_x = 0$ . Bottom: Eigenvalue braids along the BZ boundary, counterclockwise from  $(-\pi, -\pi)$ . For increasing  $t$ , the gapped phase with braids  $(B_x, B_y) = (1, \sigma_2)$  along the boundary changes to a gapped phase with braids  $(1, 1)$ . This transition is necessarily gapless, and happens via the pair-creation and winding of EP2s around the BZ.

we move these points around the BZ via the deformation  $H_s := (1-s)H_M^{\delta=1}(k_x, k_y) + sH_M^{\delta=1}(\pi, k_y)$ . We show this progression in Fig. 3 (c). For increasing  $s$ , the two EP2s move away from each other towards  $(0, \pm\pi)$ . They trace out a path cutting through the BZ and annihilate for  $s = 3/4$ . The overall difference between this fusion to a trivial degenerate point, and the previous fusion into a non-trivial braid monopole (in  $H_M^\delta$ ), is one full encircling of the torus along the  $k_x$ -direction.

By thus crossing the BZ boundary  $k_y = \pm\pi$  with increasing  $s$ , the EP2s change the corresponding boundary braid from  $B_y = \sigma_1$  to the trivial braid  $B_y = 1$ . This in turn changes the combined boundary braid enclosing the BZ to  $B_x B_y B_x^{-1} B_y^{-1} = 1\sigma_2 1\sigma_2^{-1} = 1$ . A trivial boundary braid allows for a gapped system, in accordance with our observation that the only two EP2s annihilate and vanish for  $s > 3/4$ . Hence, after encircling the torus once, the EP2s fuse into a trivial degenerate point that can be gapped out perturbatively.

The above process also suggests that pair-creation and fusion of EP2s, interspersed with topologically

non-trivial paths through the BZ, corresponds to non-Hermitian phase transitions, analogous to conversion between topologically degenerate ground states via anyons [4]. In this picture, we can label non-Hermitian topological phases by the two braids along the meridian and longitude of the BZ torus [15, 16, 20, 47] (more precisely, the conjugacy classes of these two braids in the braid group). The phase of  $H_{s=1}$  is for example denoted as  $(B_x, B_y) = (1, \sigma_2)$ . It contains an extensive Fermi arc (see Fig. 4 (a)). Taking it as a starting point, we exemplify a phase transition to the completely trivial  $(1, 1)$ -phase following the interpolation  $H_t = (1-t)H_{s=1}(k_y) + t(2 + \cos(k_x)) \text{diag}(1, 0, -1)$  for  $0 \leq t \leq 1$ . Both initial and final phase are band-gapped, with the total boundary braid  $1B_y 1B_y^{-1} = 1$  trivial. However, the two phases cannot be brought into each other immediately, since the non-trivial  $B_y$  and corresponding extensive Fermi arc persist under perturbation. Instead, a gapless topological transition that changes  $B_y$  must occur, which we show in Fig. 4. This happens via two EP2s that are pair-created at the origin  $(k_x, k_y) = (0, 0)$  (Fig. 4 (b)), and encircle

the BZ towards  $(\pm\pi, 0)$  (Fig. 4 (c)-(d)), respectively. As  $t$  increases, the two EP2s gradually destroy the Fermi arc and eventually annihilate at  $(\pm\pi, 0)$ , resulting in the trivial  $(1, 1)$ -phase without braids at all (Fig. 4 (e)).

#### IV. DISCUSSION

In this work, we have provided the first experimental realisation of a non-Abelian braid monopole. This novel degeneracy exploits a loophole in celebrated doubling theorems enabled by the highly intricate non-Abelian topology of non-Hermitian multi-band systems. We have further elucidated this topology through experimentally probing the fusion operations enabling the non-Abelian braid monopole. The experiment is facilitated by our design of new single-photon interferometric protocols, which enable the extraction of eigenstates and spectrum of highly tunable non-Hermitian Hamiltonians. Our setup opens up the possibility of simulating a wide class of topological phenomena in dissipative multi-band systems and to probe fundamental aspects of non-Abelian topology that have thus far only been subject to theoretical inquiry. The implications of these robust non-Abelian phenomena on dynamics, transport, and boundary effects are of great interest for future study.

#### ACKNOWLEDGMENTS

The authors thank Jan Carl Budich and Zhi Li for stimulating discussions. This work has been supported by the National Key R&D Program of China (Grant No. 2023YFA1406701) and National Natural Science Foundation of China (Grant Nos. 12025401, 92265209, 12374479, 12104009 and 12104036). KY is supported by the ANR-DFG project (TWISTGRAPH). JLKK and EJB were supported by the Swedish Research Council (VR, grant 2018-00313), the Wallenberg Academy Fellows program (2018.0460), and the project Dynamic Quantum Matter (2019.0068) of the Knut and Alice Wallenberg Foundation, as well as the Göran Gustafsson Foundation for Research in Natural Sciences and Medicine.

#### Appendix A: Initial state preparation

We prepare the initial state  $\rho_i$  as the completely mixed state  $\rho_i = \mathbb{1}/3$ , where  $\mathbb{1}$  is the  $3 \times 3$  identity matrix. Starting from horizontally polarised light, we first tune the polarisation of the single photons through a half-wave plate (HWP) with a setting angle of  $\cos^{-1}(\sqrt{2/3})/2 \approx 17.6^\circ$ , creating  $\sqrt{2/3}|H\rangle + \sqrt{1/3}|V\rangle$ . We then destroy the coherence between the polarisation states of the photons using an unbalanced interferometer (UBI) composed of two polarizing beam splitters (PBSs) and two mirrors [48]. Subsequently, we separate the beam into two spatial

modes, using a beam displacer (BD), which transmits vertically polarized photons into the upper spatial mode, while horizontally polarized photons undergo a 3 mm lateral displacement into the lower mode. Using another two HWPs (with setting angles of  $45^\circ$  and  $22.5^\circ$ ), and a second UBI, we destroy the coherence in the lower spatial mode. This results in the completely mixed photon state  $\rho_i$  in the space spanned by the horizontally polarised upper  $|HU\rangle$  and lower  $|HL\rangle$  modes, and the vertically polarised lower spatial mode  $|VL\rangle$ .

#### Appendix B: Realisation of non-unitary evolution

Both eigenstate preparation  $U_1$  and non-Hermitian evolution  $U_2$  are non-unitary operations. Implementing such arbitrary non-unitary evolution experimentally is challenging due to the difficulties in achieving gain in quantum systems [49, 50]. We bypass this obstacle by mapping to passive evolution without gain. For a given evolution  $\tilde{U}(\tau)$  with gain, we map to  $U = \tilde{U}(\tau)e^{-\Lambda(\tau)}$ . We choose  $\Lambda(\tau) = \ln \sqrt{\max_j |\lambda_j|}$ , where  $\lambda_j$  are the eigenvalues of  $\tilde{U}(\tau)\tilde{U}^\dagger(\tau)$ . Under this mapping, gain terms are converted to no loss, and loss terms to even greater loss, leading to a passive operation  $U$  [51–53].

We implement such passive non-unitary evolution  $U$  using its singular-value decomposition  $U = VDW$  [54]. Here, the operator  $D$  is a non-unitary diagonal matrix with the first diagonal element  $D_{11} = 1$ , and the rest less than 1 (see Fig. 1). It is realized by introducing mode-selective losses of photons by adjusting the angles of  $H_1$  and  $H_2$  shown in Fig. 1. The unitary operations of  $W$  and  $V$  can be further decomposed as  $W = W_{12}W_{13}W_{23}$  and  $V = V_{23}V_{13}V_{12}$ , such that the unitary operators  $W_{ij}$  and  $V_{ij}$  only act on a two-dimensional subspace of the qutrit system [55]. We realise them by combining photons from different hybrid modes into a certain spatial mode, and then applying the transformation through wave plates.

#### Appendix C: Eigenstate Extraction

We purify the initial mixed state  $\rho_i$  into a right eigenstate  $|R_j\rangle$  of  $H(\mathbf{k})$  using an appropriately chosen non-unitary evolution  $U_1 = e^{f_j(H)\tau_1}$ . As a concrete example, we prepare the eigenstate  $|R_1\rangle$  with the greatest real part of the energy, using the imaginary-time evolution governed by  $f_1(H) = H$ . The corresponding evolution operator is

$$U_1 = e^{H\tau_1} = \sum_j e^{E_j\tau_1} \Pi_j, \quad (\text{C1})$$

where  $E_j$  are the eigenvalues of  $H$ , and  $\Pi_j$  are the projectors to the corresponding eigenspace, satisfying  $\Pi_j \Pi_k = \delta_{jk} \Pi_k$  and  $\sum_j \Pi_j = \mathbb{1}$ . The projectors can be expressed as  $\Pi_j = |R_j\rangle \langle L_j| / \langle L_j | R_j \rangle$  in terms of the corresponding right (left) eigenstates  $|R_j\rangle$  ( $\langle L_j|$ ) of

$H$ , when we are not exactly at the EPs. These eigenstates satisfy  $\langle L_j | R_k \rangle_{j \neq k} = 0$ , and we normalise them as  $\langle L_j | L_j \rangle = \langle R_j | R_j \rangle = 1$ . We write the eigenvalues' real and imaginary parts as  $E_j = E_j^R + iE_j^I$ , and sort them such that for  $j < k$ ,  $E_j^R > E_k^R$  without loss of generality.

After evolving under  $U_1$ , the initial state  $\rho_i$  becomes

$$\rho_{\tau_1} = U_1(\tau_1)\rho_i U_1^\dagger(\tau_1) = \sum_{j,k} e^{\tau_1(E_j + E_k^*)} \frac{c_{jk}}{3} |R_j\rangle\langle R_k|, \quad (\text{C2})$$

where  $c_{jk} = \langle L_j | L_k \rangle / (\langle L_j | R_j \rangle \langle R_k | L_k \rangle)$ . The exponential  $e^{\tau_1(E_j + E_k^*)} = e^{(E_j^R + E_k^R)\tau_1} e^{i(E_j^I - E_k^I)\tau_1}$  damps all eigenstates relative to  $|R_1\rangle$ , which corresponds to the eigenvalue with largest real part, and which is therefore the steady state.

Likewise, by using  $f_3(H) = -H$  in  $U_1$ , we obtain as the steady state  $|R_3\rangle$ , which has the lowest real eigenvalues of  $E_3^R$ . To determine the eigenstate  $|R_2\rangle$ , we must first determine the eigenvalues of  $E_1$  and  $E_3$  by interferometric measurements. Once  $E_1$  and  $E_3$  are known, we can formulate a new Hamiltonian  $\tilde{H} = [H - \frac{E_1 + E_3}{2} \mathbb{1}]^2$ . While this retains the same eigenstates, the real components of the corresponding eigenvalues of  $|R_1\rangle$  and  $|R_3\rangle$  both become  $[(E_3^R - E_1^R)^2 - (E_3^I - E_1^I)^2]/4$ . Consequently, we can obtain  $|R_2\rangle$  as the steady pure state of the imaginary time evolution governed by  $f_2(H) = -\tilde{H}$  or  $f_2(H) = \tilde{H}$ . To purify the evolved states with high fidelity, we fix the evolution time  $\tau_1 = 10$  for the eigenstate extraction.

#### Appendix D: Eigenvalue Measurement

The single photons, prepared in the eigenstate  $|R_j\rangle$  are injected into a non-polarizing beam splitter (NPBS). This splits the beam into another two spatial modes, transmitted  $|t\rangle$  and reflected  $|r\rangle$ . We apply the non-unitary operation  $U_2 = e^{-i(H - i\Lambda \mathbb{1})\tau_2}$  on the photons in the transmitted mode  $|t\rangle$ , while leaving those in  $|r\rangle$  unchanged. The state then evolves to  $(e^{-i\tilde{E}_j\tau_2} |t\rangle |R_j\rangle + |r\rangle |R_j\rangle) / \sqrt{2}$ , where  $\tilde{E}_j = E_j - i\Lambda$ . Without loss of generality, we fix  $\tau_2 = 1$  for  $U_2$ .

Subsequently, we perform interferometric measurements to obtain the eigenvalues  $E_j$  of  $H(\mathbf{k})$  [52]. We achieve this by first applying a HWP at  $45^\circ$  to the transmitted photons. Then, the transmitted and reflected photons are recombined using a PBS. Thereby, a generic state  $|R_j\rangle = \alpha_j |H_U\rangle + \beta_j |H_L\rangle + \gamma_j |V_L\rangle$  evolves into

$$\begin{aligned} |R'_j\rangle &= \frac{1}{\sqrt{2}} (\alpha_j |t'U\rangle + \beta_j |t'L\rangle) \left( |H\rangle + e^{-i\tilde{E}_j} |V\rangle \right) \\ &+ \frac{1}{\sqrt{2}} \gamma_j |r'L\rangle \left( e^{-i\tilde{E}_j} |H\rangle + |V\rangle \right). \end{aligned} \quad (\text{D1})$$

Here,  $|t'\rangle$  and  $|r'\rangle$  denote the transmitted (reflected) modes after passing the photons reflected by the NPBS through the second PBS.

Finally, we measure the complex phase through successive projective measurements on the polarisation states  $\{|\pm\rangle = (|H\rangle \pm |V\rangle) / \sqrt{2}, |\odot\rangle = (|H\rangle - i|V\rangle) / \sqrt{2}\}$  in the different spatial modes. Measuring, e.g., coincidence counts  $N_{t'U}^+$  for the state  $|+, t'U\rangle$ , normalised to the total number  $N_{\text{tot}}$  of input photons after purification, leads to

$$\begin{aligned} \frac{N_{t'U}^+}{N_{\text{tot}}} &= |\langle t'U, + | R'_j \rangle|^2 \\ &= \left| \frac{\alpha_j}{2} (1 + e^{-i\tilde{E}_j}) \right|^2 \\ &= \frac{|\alpha_j|^2}{2} \left( \frac{1 + e^{2\text{Im}(\tilde{E}_j)}}{2} + \frac{e^{-i\tilde{E}_j} + e^{i\tilde{E}_j}}{2} \right). \end{aligned} \quad (\text{D2})$$

The linear combination

$$\begin{aligned} \xi_j &= \left[ \left( (i+1) \frac{N_{t'U}^+}{N_{\text{tot}}} + (i-1) \frac{N_{t'U}^-}{N_{\text{tot}}} - 2i \frac{N_{t'U}^\odot}{N_{\text{tot}}} \right) \right. \\ &+ \left( (i+1) \frac{N_{r'L}^+}{N_{\text{tot}}} + (i-1) \frac{N_{r'L}^-}{N_{\text{tot}}} - 2i \frac{N_{r'L}^\odot}{N_{\text{tot}}} \right) \\ &\left. + \left( (1-i) \frac{N_{r'L}^+}{N_{\text{tot}}} - (i+1) \frac{N_{r'L}^-}{N_{\text{tot}}} + 2i \frac{N_{r'L}^\odot}{N_{\text{tot}}} \right) \right]. \end{aligned} \quad (\text{D3})$$

of such coincidence counts equals  $\xi_j = \langle R'_j | U_2 | R'_j \rangle$ , from which we finally obtain the eigenvalues of  $H(\mathbf{k})$  with

$$E_j = \tilde{E}_j + i\Lambda = i \ln(\xi_j) + i\Lambda. \quad (\text{D4})$$

#### Appendix E: Splitting of the monopole.

When the parameter  $\delta$  in  $H_M^\delta$  is tuned to be less than  $1 + 2\sqrt{2}$ , the monopole splits into a pair of twofold exceptional points (EP2s). Figure 5 illustrates that with the decrease of  $\delta$  to 1.5 and 1, these EP2s can be found at  $(k_x, k_y) \approx \pm(0.231, -0.231)$  and  $(k_x, k_y) \approx \pm(0.815, -0.815)$ , respectively. It is noticeable that as  $\delta$  decreases, the pair of EP2s move away from each other along the line of  $k_x = -k_y$  [25]. Moreover, with the decrease of  $\delta$ , the two Fermi arcs (signify the closure of one of the real energy gaps  $\text{Re}(E_i - E_j) = 0$  [56]) intersecting at the monopole split to cross each EP2. The imaginary-Fermi arc (representing the closure of one of the imaginary energy gaps) along  $k_x = -k_y$  is separated by a new emerging Fermi arc that terminates at EP2s. In Figs. 5(b) and (d), we show the measured real and imaginary parts of the bands along these Fermi and i-Fermi arcs, illustrating splitting of the monopole.

When encircling an exceptional point along a counter-clockwise path, the eigenenergies start to evolve around each other. This pattern forms a braid on the eigenenergies. If the path can be constructed by consecutive loops, the total braid pattern is the product of the braids around each loop. This establishes a natural correspondence between exceptional points and braid patterns, where each exceptional point can be associated with an element in

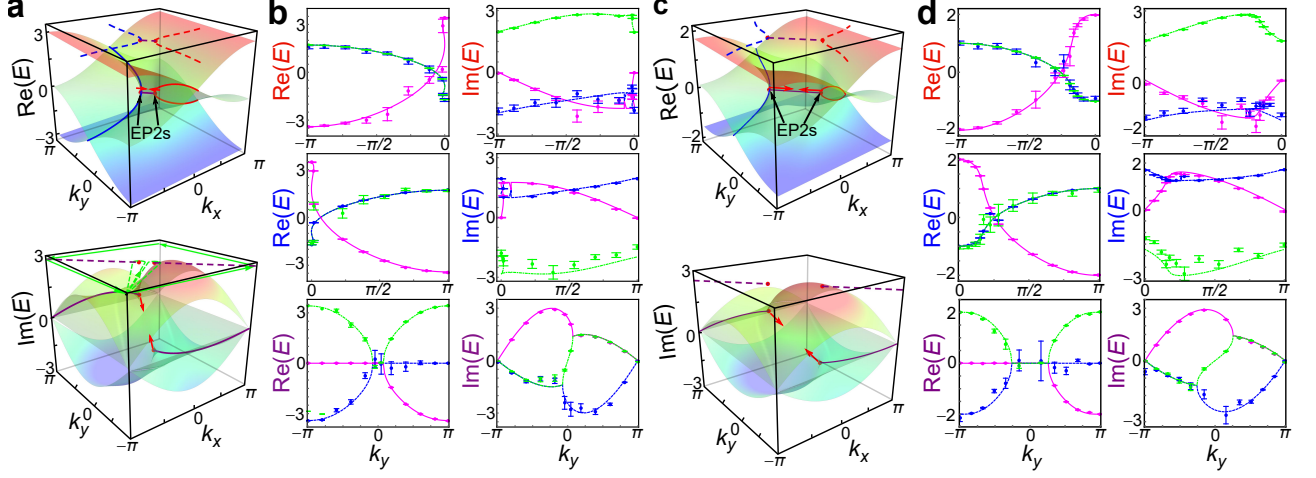


FIG. 5. Observation of Fermi and i-Fermi arcs in  $H_M^\delta$ . Theoretical results for the real and imaginary parts of the eigenenergies of  $H_M^\delta$  with (a)  $\delta = 1.5$  and (c)  $\delta = 1$ , shown as colored surfaces over the Brillouin zone (BZ). The red dots correspond to the twofold exceptional points (EP2s). The solid lines depict both the Fermi arcs of the real eigenenergy components and the i-Fermi arcs of the imaginary components. The dashed lines are their projections on the  $k_x - k_y$  plane. Measured complex eigenenergies along the Fermi and i-Fermi arcs drawn in (a) and (c) are presented in (b) and (d), respectively. Experimental data are presented by symbols, while theoretical predictions are denoted by colored lines. Error bars indicate the statistical uncertainty, which are obtained by assuming Poisson statistics in the photon-number fluctuations.

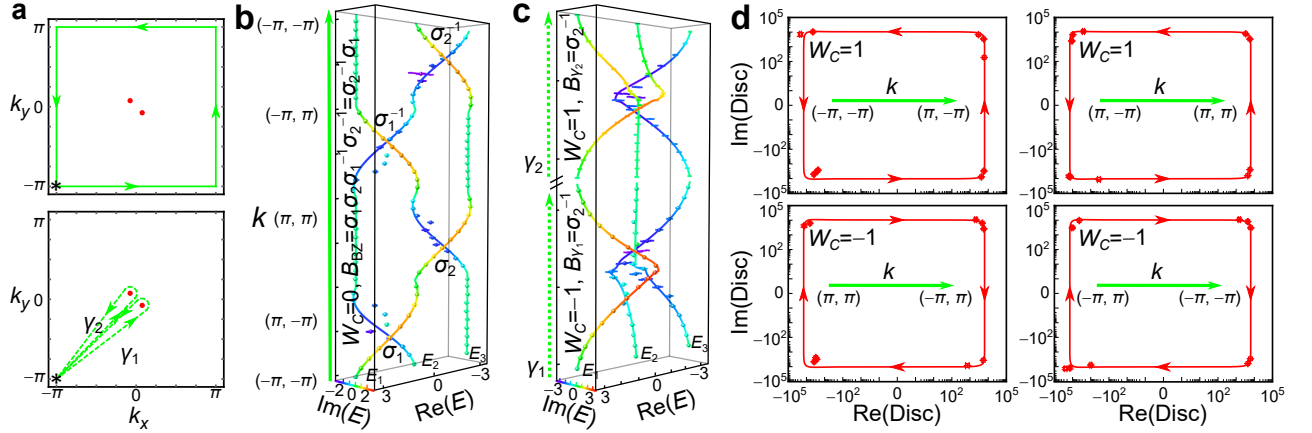


FIG. 6. The braids in  $H_M^\delta$  with  $\delta = 1.5$ . (a) Parametric loops along the BZ boundary (green solid line in the top panel) and EP2s of  $\gamma_{1,2}$  (green dashed lines in the down panel). Exceptional points are represented by the red dots. The corresponding measured braids are shown in (b) and (c), respectively. (d) Measured discriminant for the four segments along the boundary of BZ. Experimental data are presented by symbols, while theoretical predictions are denoted by colored lines. Error bars indicate the statistical uncertainty, which are obtained by assuming Poisson statistics in the photon-number fluctuations.

the braid group [15, 16, 57, 58]. For a general  $N$ -band non-Hermitian system, the eigenenergies can be sorted as  $\text{Re}(E_j) \geq \text{Re}(E_{j+1})$ . The braid group is constructed by the braids  $\sigma_j$  ( $\sigma_j^{-1}$ ) ( $1 \leq j \leq N-1$ ), which swap  $E_j$  and  $E_{j+1}$  counterclockwise (clockwise) in the complex plane. They satisfy the braid relations [33, 59]

$$\sigma_j \sigma_{j+1} \sigma_j = \sigma_{j+1} \sigma_j \sigma_{j+1}, \quad \sigma_i \sigma_j = \sigma_j \sigma_i \quad (|i-j| > 1). \quad (\text{E1})$$

As shown in Figs. 2(c) and (d), we measure the braids of the monopole along the loops of  $\gamma$  and the boundary of the BZ. They can be represented by  $\sigma_1 \sigma_2 \sigma_1^{-1} \sigma_2^{-1}$ , where the deformations of the loop do not alter the braid. Ac-

cording to the braid relations in Eq. E1, these braids can also be rewritten as,

$$\sigma_1 \sigma_2 \sigma_1^{-1} \sigma_2^{-1} = \sigma_2^{-1} (\sigma_1 \sigma_2 \sigma_1) \sigma_1^{-1} \sigma_2^{-1} = \sigma_2^{-1} \sigma_1. \quad (\text{E2})$$

As shown in Fig. 6 and Fig. 3(b), the splitting of the monopole by tuning the on-site potential to  $\delta = 1.5$  and  $\delta = 1$  do not alter the braid along the boundary of the BZ.

Additionally, we measure the braid patterns when encircling each of the EP2s, observing that the braids are topologically invariant as  $\delta$  decrease. Specifically, the EP2s at  $(k_x \approx 0.231, k_y \approx -0.231)$  for  $\delta = 1.5$  and

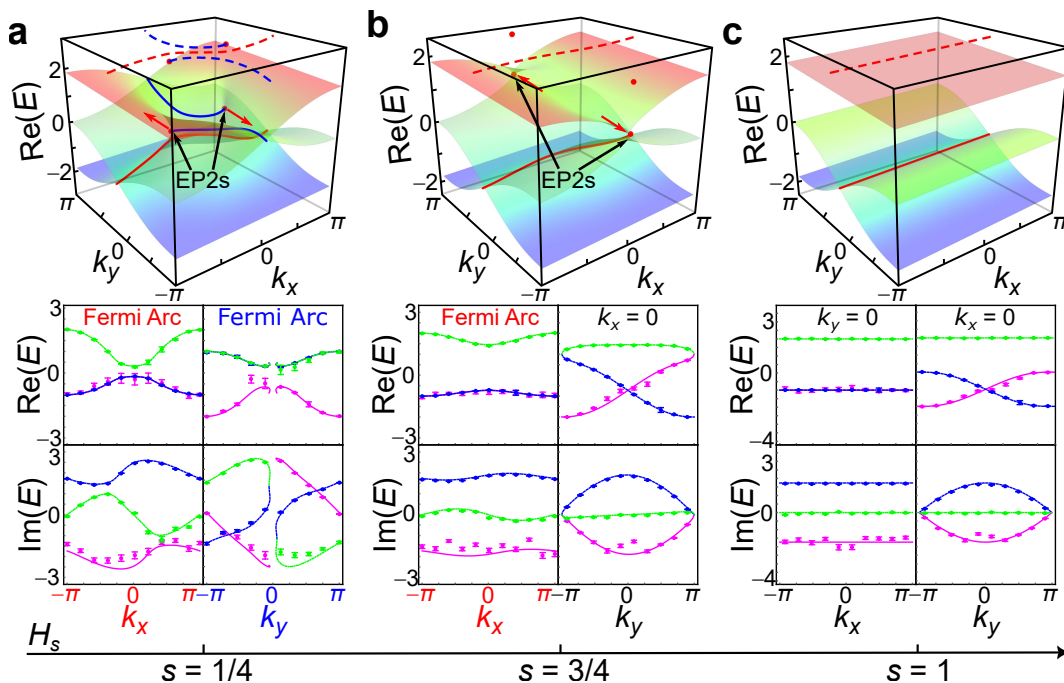


FIG. 7. Observation of the eigenenergies of  $H_s$ . The measured real and imaginary parts of the bands of  $H_s$  with  $s = 1/4$  (a),  $s = 3/4$  (b) and  $s = 1$  (c). Top: Theoretical results for the real and imaginary parts of the eigenenergies, shown as colored surfaces over the BZ. The red dots correspond to EP2s. The solid lines depict the Fermi arcs. The dashed lines are their projections on the  $k_x - k_y$  plane. Bottom: Measured complex eigenenergies along the Fermi arcs or  $k_x = 0$  and  $k_y = 0$ . Experimental data are presented by symbols, while theoretical predictions are denoted by colored lines. Error bars indicate the statistical uncertainty, which are obtained by assuming Poisson statistics in the photon-number fluctuations.

( $k_x \approx 0.815, k_y \approx -0.815$ ) for  $\delta = 1$  braid the second two eigenenergies clockwise along path  $\gamma_1$ . Differently, the EP2s located at ( $k_x \approx -0.231, k_y \approx 0.231$ ) and ( $k_x \approx -0.815, k_y \approx 0.815$ ) braid the first two eigenenergies counterclockwise along  $\gamma_2$ . Consequently, the braids of EP2s exhibit the non-Abelian braids of  $\sigma_2^{-1}$  and  $\sigma_1$  [60], compensating the boundary braids (see Eq. (E2)) as per the non-Abelian sum rule. The corresponding winding numbers of these braids are  $\mp 1$  for  $\gamma_{1,2}$

and 0 along the boundary of BZ.

Figure 7 illustrates the measured Fermi arcs in  $H_s$  with the increasing of  $s$ . The initial model  $H_{s=0} = H_{\delta=1}^M$  (shown in Figs. 5(c) and (d)) hosts two topologically non-trivial Fermi arcs, each along a great circle. For increasing  $s$ , these two Fermi arcs are cleaved into three segments by the exceptional points. Upon the annihilation of the EP2s with  $s > 3/4$ , two of the Fermi arcs, terminated by exceptional points, are eliminated from the Brillouin zone.

- 
- [1] Paul Adrien Maurice Dirac, “Quantised singularities in the electromagnetic field,” *Proc. R. Soc. A* **133**, 60–72 (1997).
  - [2] H.B. Nielsen and M. Ninomiya, “Absence of neutrinos on a lattice: (I). Proof by homotopy theory,” *Nucl. Phys. B* **185**, 20–40 (1981).
  - [3] H.B. Nielsen and M. Ninomiya, “Absence of neutrinos on a lattice: (II). Intuitive topological proof,” *Nucl. Phys. B* **193**, 173–194 (1981).
  - [4] Chetan Nayak, Steven H. Simon, Ady Stern, Michael Freedman, and Sankar Das Sarma, “Non-Abelian anyons and topological quantum computation,” *Rev. Mod. Phys.* **80**, 1083–1159 (2008).
  - [5] M.V. Berry, “Physics of non-Hermitian degeneracies,” *Czech. J. Phys.* **54**, 1039–1047 (2004).
  - [6] W. D. Heiss, “The physics of exceptional points,” *J. Phys. A: Math. Theor.* **45**, 444016 (2012).
  - [7] Haitan Xu, David Mason, Luyao Jiang, and JGE Harris, “Topological energy transfer in an optomechanical system with exceptional points,” *Nature* **537**, 80–83 (2016).
  - [8] Jörg Doppler, Alexei A Mailybaev, Julian Böhm, Ulrich Kuhl, Adrian Girschik, Florian Libisch, Thomas J Milburn, Peter Rabl, Nimrod Moiseyev, and Stefan Rotter, “Dynamically encircling an exceptional point for asymmetric mode switching,” *Nature* **537**, 76–79 (2016).
  - [9] Hossein Hodaei, Absar U Hassan, Steffen Wittek, Hipolito Garcia-Gracia, Ramy El-Ganainy, Demetrios N Christodoulides, and Mercedeh Khajavikhan, “Enhanced sensitivity at higher-order exceptional points,” *Nature* **548**, 187–191 (2017).

- [10] Weijian Chen, Sahin Kaya Özdemir, Guangming Zhao, Jan Wiersig, and Lan Yang, “Exceptional points enhance sensing in an optical microcavity,” *Nature* **548**, 192–196 (2017).
- [11] Qi Zhong, Mercedeh Khajavikhan, Demetrios N Christodoulides, and Ramy El-Ganainy, “Winding around non-Hermitian singularities,” *Nat. Commun.* **9**, 4808 (2018).
- [12] M Naghiloo, M Abbasi, Yogesh N Joglekar, and KW Murch, “Quantum state tomography across the exceptional point in a single dissipative qubit,” *Nat. Phys.* **15**, 1232–1236 (2019).
- [13] Yuto Ashida, Zongping Gong, and Masahito Ueda, “Non-Hermitian physics,” *Adv. Phys.* **69**, 249–435 (2020).
- [14] Emil J. Bergholtz, Jan Carl Budich, and Flore K. Kunst, “Exceptional topology of non-Hermitian systems,” *Rev. Mod. Phys.* **93**, 015005 (2021).
- [15] Charles C. Wojcik, Xiao-Qi Sun, Tomáš Bzdušek, and Shanhui Fan, “Homotopy characterization of non-Hermitian Hamiltonians,” *Phys. Rev. B* **101**, 205417 (2020).
- [16] Zhi Li and Roger S. K. Mong, “Homotopical characterization of non-Hermitian band structures,” *Phys. Rev. B* **103**, 155129 (2021).
- [17] Haiping Hu and Erhai Zhao, “Knots and non-Hermitian Bloch bands,” *Phys. Rev. Lett.* **126**, 010401 (2021).
- [18] Kai Wang, Avik Dutt, Charles C. Wojcik, and Shanhui Fan, “Topological complex-energy braiding of non-Hermitian bands,” *Nature* **598**, 59–64 (2021).
- [19] Yogesh S. S. Patil, Judith Höller, Parker A. Henry, Chitres Guria, Yiming Zhang, Luyao Jiang, Nenad Kralj, Nicholas Read, and Jack G. E. Harris, “Measuring the knot of non-Hermitian degeneracies and non-commuting braids,” *Nature* **607**, 271–275 (2022).
- [20] Kang Yang, Zhi Li, J. Lukas K. König, Lukas Rødland, Marcus Stålhammar, and Emil J. Bergholtz, “Homotopy, symmetry, and non-Hermitian band topology,” *Rep. Prog. Phys.* **87**, 078002 (2024).
- [21] Jie Ren and N. A. Sinitsyn, “Braid group and topological phase transitions in nonequilibrium stochastic dynamics,” *Phys. Rev. E* **87**, 050101 (2013).
- [22] Eric J. Pap, Daniël Boer, and Holger Waalkens, “Non-Abelian nature of systems with multiple exceptional points,” *Phys. Rev. A* **98**, 023818 (2018).
- [23] Yi Yang, Biao Yang, Guancong Ma, Jensen Li, Shuang Zhang, and CT Chan, “Non-Abelian physics in light and sound,” *Science* **383**, eadf9621 (2024).
- [24] Linhu Li, Ching Hua Lee, Sen Mu, and Jiangbin Gong, “Critical non-Hermitian skin effect,” *Nat. Commun.* **11**, 5491 (2020).
- [25] J. Lukas K. König, Kang Yang, Jan Carl Budich, and Emil J. Bergholtz, “Braid-protected topological band structures with unpaired exceptional points,” *Phys. Rev. Research* **5**, L042010 (2023).
- [26] Mohammad-Ali Miri and Andrea Alù, “Exceptional points in optics and photonics,” *Science* **363**, eaar7709 (2019).
- [27] Şahin Kaya Özdemir, Stefan Rotter, Franco Nori, and L Yang, “Parity–time symmetry and exceptional points in photonics,” *Nat. Mater.* **18**, 783–798 (2019).
- [28] C. Dembowski, H.-D. Gräf, H. L. Harney, A. Heine, W. D. Heiss, H. Rehfeld, and A. Richter, “Experimental observation of the topological structure of exceptional points,” *Phys. Rev. Lett.* **86**, 787–790 (2001).
- [29] Kun Ding, Guancong Ma, Meng Xiao, Z. Q. Zhang, and C. T. Chan, “Emergence, coalescence, and topological properties of multiple exceptional points and their experimental realization,” *Phys. Rev. X* **6**, 021007 (2016).
- [30] Hengyun Zhou, Chao Peng, Yoseob Yoon, Chia Wei Hsu, Keith A. Nelson, Liang Fu, John D. Joannopoulos, Marin Soljačić, and Bo Zhen, “Observation of bulk Fermi arc and polarization half charge from paired exceptional points,” *Science* **359**, 1009–1012 (2018).
- [31] Wei Wang, Xulong Wang, and Guancong Ma, “Non-Hermitian morphing of topological modes,” *Nature* **608**, 50–55 (2022).
- [32] Qicheng Zhang, Yitong Li, Huanfa Sun, Xun Liu, Luekai Zhao, Xiling Feng, Xiyang Fan, and Chunyin Qiu, “Observation of acoustic non-Hermitian Bloch braids and associated topological phase transitions,” *Phys. Rev. Lett.* **130**, 017201 (2023).
- [33] Qicheng Zhang, Luekai Zhao, Xun Liu, Xiling Feng, Liwei Xiong, Wenquan Wu, and Chunyin Qiu, “Experimental characterization of three-band braid relations in non-Hermitian acoustic lattices,” *Phys. Rev. Research* **5**, L022050 (2023).
- [34] Jia-Zheng Li, Kai Bai, Cheng Guo, Tian-Rui Liu, Liang Fang, Duanduan Wan, and Meng Xiao, “Braiding topology of symmetry-protected degeneracy points in non-Hermitian systems,” *Phys. Rev. B* **109**, L041102 (2024).
- [35] Chitres Guria, Qi Zhong, Sahin Kaya Ozdemir, Yogesh S. S. Patil, Ramy El-Ganainy, and Jack Gwynne Emmet Harris, “Resolving the topology of encircling multiple exceptional points,” *Nat. Commun.* **15**, 1369 (2024).
- [36] Ady Stern, “Non-Abelian states of matter,” *Nature* **464**, 187–193 (2010).
- [37] QuanSheng Wu, Alexey A Soluyanov, and Tomáš Bzdušek, “Non-Abelian band topology in noninteracting metals,” *Science* **365**, 1273–1277 (2019).
- [38] Adrien Bouhon, QuanSheng Wu, Robert-Jan Slager, Hongming Weng, Oleg V Yazyev, and Tomáš Bzdušek, “Non-Abelian reciprocal braiding of Weyl points and its manifestation in ZrTe,” *Nat. Phys.* **16**, 1137–1143 (2020).
- [39] Dongyang Wang, Ying Wu, Z. Q. Zhang, and C. T. Chan, “Non-Abelian frame charge flow in photonic media,” *Phys. Rev. X* **13**, 021024 (2023).
- [40] Mario Motta, Chong Sun, Adrian TK Tan, Matthew J O’Rourke, Erika Ye, Austin J Minnich, Fernando GSL Brandao, and Garnet Kin-Lic Chan, “Determining eigenstates and thermal states on a quantum computer using quantum imaginary time evolution,” *Nat. Phys.* **16**, 205–210 (2020).
- [41] Sam McArdle, Tyson Jones, Suguru Endo, Ying Li, Simon C Benjamin, and Xiao Yuan, “Variational ansatz-based quantum simulation of imaginary time evolution,” *npj Quantum Inf.* **5**, 75 (2019).
- [42] Zhesen Yang, A. P. Schnyder, Jiangping Hu, and Ching-Kai Chiu, “Fermion doubling theorems in two-dimensional non-Hermitian systems for Fermi points and exceptional points,” *Phys. Rev. Lett.* **126**, 086401 (2021).
- [43] Charles C. Wojcik, Kai Wang, Avik Dutt, Janet Zhong, and Shanhui Fan, “Eigenvalue topology of non-Hermitian band structures in two and three dimensions,” *Phys. Rev. B* **106**, L161401 (2022).
- [44] Haiping Hu, Shikang Sun, and Shu Chen, “Knot topology of exceptional point and non-Hermitian no-go theo-

- rem,” *Phys. Rev. Research* **4**, L022064 (2022).
- [45] Daniel Leykam, Konstantin Y. Bliokh, Chunli Huang, Y. D. Chong, and Franco Nori, “Edge modes, degeneracies, and topological numbers in non-Hermitian systems,” *Phys. Rev. Lett.* **118**, 040401 (2017).
- [46] Raoul Bott and Loring W Tu, *Differential Forms in Algebraic Topology*, Vol. 82 (Springer New York, NY, 1982).
- [47] Huitao Shen, Bo Zhen, and Liang Fu, “Topological band theory for non-Hermitian Hamiltonians,” *Phys. Rev. Lett.* **120**, 146402 (2018).
- [48] Wen-Hao Zhang, Geng Chen, Xing-Xiang Peng, Xiang-Jun Ye, Peng Yin, Ya Xiao, Zhi-Bo Hou, Ze-Di Cheng, Yu-Chun Wu, Jin-Shi Xu, Chuan-Feng Li, and Guang-Can Guo, “Experimentally robust self-testing for bipartite and tripartite entangled states,” *Phys. Rev. Lett.* **121**, 240402 (2018).
- [49] Ze-Guo Chen, Ruo-Yang Zhang, C. T. Chan, and Guancong Ma, “Classical non-Abelian braiding of acoustic modes,” *Nat. Phys.* **18**, 179–184 (2022).
- [50] Stefano Longhi, “Parity-time symmetry meets photonics: A new twist in non-Hermitian optics,” *EuroPhys. Lett.* **120**, 64001 (2018).
- [51] Kunkun Wang, Lei Xiao, Jan Carl Budich, Wei Yi, and Peng Xue, “Simulating exceptional non-Hermitian metals with single-photon interferometry,” *Phys. Rev. Lett.* **127**, 026404 (2021).
- [52] Kunkun Wang, Lei Xiao, Haiqing Lin, Wei Yi, Emil J. Bergholtz, and Peng Xue, “Experimental simulation of symmetry-protected higher-order exceptional points with single photons,” *Sci. Adv.* **9**, eadi0732 (2023).
- [53] Rui Ye, Yanyan He, Guangzhen Li, Luojia Wang, Xiaoxiong Wu, Xin Qiao, Yuanlin Zheng, Liang Jin, Da-Wei Wang, Luqi Yuan, and Xianfeng Chen, “Observation of non-Hermitian antichiral edge currents,” Preprint at <https://arxiv.org/abs/2305.17853> (2023).
- [54] N. Tischler, C. Rockstuhl, and K. Slowik, “Quantum optical realization of arbitrary linear transformations allowing for loss and gain,” *Phys. Rev. X* **8**, 021017 (2018).
- [55] Michael Reck, Anton Zeilinger, Herbert J. Bernstein, and Philip Bertani, “Experimental realization of any discrete unitary operator,” *Phys. Rev. Lett.* **73**, 58–61 (1994).
- [56] Mu Yang, Hao-Qing Zhang, Yu-Wei Liao, Zheng-Hao Liu, Zheng-Wei Zhou, Xing-Xiang Zhou, Jin-Shi Xu, Yong-Jian Han, Chuan-Feng Li, and Guang-Can Guo, “Realization of exceptional points along a synthetic orbital angular momentum dimension,” *Sci. Adv.* **9**, eabp8943 (2023).
- [57] Cui-Xian Guo, Shu Chen, Kun Ding, and Haiping Hu, “Exceptional non-Abelian topology in multiband non-Hermitian systems,” *Phys. Rev. Lett.* **130**, 157201 (2023).
- [58] K Ding, C. Fang, and G. Ma, “Non-Hermitian topology and exceptional-point geometries,” *Nat. Rev. Phys.* **4**, 745–760 (2022).
- [59] C. Kassel and V. Turaev, *Braid Groups* (Springer New York, NY, 2008).
- [60] Yang Long, Zihao Wang, Chen Zhang, Haoran Xue, Y. X. Zhao, and Baile Zhang, “Non-Abelian braiding of topological edge bands,” *Phys. Rev. Lett.* **132**, 236401 (2024).